Reprinted from THE JOURNAL of the Acoustical Society of America

Vol. 84, No. 6, December 1988

The time-domain solution of the wide-angle parabolic equation including the effects of sediment dispersion

Michael D. Collins
Naval Ocean Research and Development Activity, Stennis Space Center, Mississippi 39529

pp. 2114-2125

The time-domain solution of the wide-angle parabolic equation including the effects of sediment dispersion

Michael D. Collins
Naval Ocean Research and Development Activity, Stennis Space Center, Mississippi 39529

(Received 8 March 1988; accepted for publication 10 August 1988)

The wide-angle time-domain parabolic equation (TDPE), which is the inverse Fourier transform of the wide-angle parabolic equation (PE), is derived. A numerical solution for the model is described and a benchmark calculation is presented. The narrow-angle TDPE is also considered and its error is analyzed and compared with the error of the narrow-angle PE. The TDPE is compared with the progressive wave equation, which is shown to be restricted to narrow-angle propagation for practical purposes. In the sediment, attenuation is assumed to depend linearly on frequency and the corresponding causal dispersion law is assumed. The model is used to show that the effect of sediment dispersion on pulse propagation in the ocean can be significant.

PACS numbers: 43.30.Bp, 43.30.Ma, 43.20.Bi

INTRODUCTION

Time-domain approaches are useful for modeling broadband acoustic propagation. For example, suppose that a sequence of snapshots of the acoustic pressure in two spatial variables is desired to study the evolution of a pulse in time. With frequency-domain approaches to this problem, it is necessary to: (a) Fourier decompose the source function; (b) solve the propagation problem for each frequency; (c) store and manage the solution for each frequency; and (d) perform a three-way sum over frequency and space for each snapshot. Errors due to approximations and round-off occur in steps (a), (b), and (d). Step (a) requires the selection of a frequency spacing and a frequency band. Step (b) requires the selection of grid spacings for each frequency. Step (c) can be difficult for broadband problems. Even if step (b) requires less computer time (CPU) than a time-domain calculation, it is possible that step (d) will offset the advantage. For an analogous problem,[1] inverting a modal decomposition required several times as much CPU as performing the calculation for each of the modes.

In shallow water, it is essential for an underwater pulse propagation model to handle bottom interaction, range-dependence, and wide-angle propagation. Since the ocean is an inhomogeneous waveguide of variable depth, a realistic propagation model must handle both bottom interaction and range dependence. Benchmark studies[2] indicate that wide-angle capability is important in underwater acoustic modeling. The parabolic equation[3] (PE) method is ideally suited to handle range dependence. With the development of wide-angle capability,[4,5] the PE method became the most useful frequency-domain tool available for bottom-interacting propagation. Two time-domain methods related to the PE method have been developed. The progressive wave equation[6-8] (PWE) advances the acoustic pressure in time. The PWE has been extended to handle nonlinear propagation[7] and bottom interaction.[8] The time-domain parabolic equation[6,9] (TDPE) is the inverse Fourier transform of the PE. It advances the acoustic pressure in range. More effort has gone into the development of the PWE, perhaps because it is more natural to march a solution of the wave equation in time rather than range.

In this article, the TDPE is extended to handle wide-angle propagation, and an energy argument is presented that shows that the PWE is not useful for wide-angle propagation. A benchmark calculation is presented and the error of the narrow-angle TDPE is compared with the error of the narrow-angle PE. Sediment attenuation is assumed to depend linearly on frequency, which agrees with experimental results involving various materials and frequencies.[10-12] The corresponding causal sediment dispersion relation,[13] which has been validated experimentally,[11] is also assumed in the sediment. A calculation is presented to demonstrate that sediment dispersion can have a significant effect on pulse propagation in the ocean.

I. THE FREQUENCY-DOMAIN PARABOLIC EQUATION

A time-harmonic steady state is assumed and the acoustic pressure p is factored as $p(\mathbf{x},t) = P(\mathbf{x})\exp(-i\omega t)$, where t is time, $\mathbf{x}$ is the Cartesian position vector, and ω is the circular frequency. The complex pressure P is assumed to satisfy the pressure-release boundary condition $P = 0$ at the ocean surface, the outgoing radiation condition at infinity, and the reduced wave equation[14]

$$\rho\nabla\cdot[(1/\rho)\nabla P] + K^2 P = -4\pi\delta(\mathbf{x}-\mathbf{x}_0), \qquad (1)$$

where the point $\mathbf{x}_0$ is the source location. The complex wavenumber $K = k + i\sigma\beta|k|$ is used to account for sediment loss. Absolute value is used so that energy loss occurs in the direction of propagation. The wavenumber is $k = \omega/c$, $\sigma = (40\pi\log_{10}e)^{-1}$, β is the attenuation in decibels per wavelength (dB/λ), ρ is the density, and c is the sound speed. The variable density term is due to Bergmann.[15]

To reduce to two spatial dimensions, we assume that azimuthal variations are negligible. Since the ocean is a waveguide, energy propagating from a source exhibits cylin-

 0001-4966/88/122114-12$00.80

drical spreading. Thus it is often beneficial to solve Eq. (1) in cylindrical coordinates with z being the depth below the ocean surface and r being the horizontal distance from a source at the depth z_0. Variations in range are assumed to be sufficiently weak so that $\partial\rho/\partial r$ can be ignored, which simplifies Eq. (1) to

$$\frac{\partial^2 P}{\partial z^2} - \frac{1}{\rho}\frac{\partial \rho}{\partial z}\frac{\partial P}{\partial z} + \frac{\partial^2 P}{\partial r^2} + \frac{1}{r}\frac{\partial P}{\partial r} + K^2 P = -(2/r)\,\delta(r)\delta(z - z_0). \tag{2}$$

The propagation angle of a ray is defined to be the angle it makes with the ocean surface. We define α_M to be the maximum angle of propagation in the ocean.[16] Rays that propagate with angles greater than α_M are not trapped in the ocean and thus do not contribute to the farfield. Since the discontinuity in sound speed at the ocean bottom is small, $\epsilon = \tan^2 \alpha_M \ll 1$ and $k_0^{-1}|k - k_0| = O(\epsilon)$, where k_0 is an average wavenumber in the water column. We define $Q = r^{1/2}P$, and Eq. (2) becomes

$$\frac{\partial^2 Q}{\partial z^2} - \frac{1}{\rho}\frac{\partial \rho}{\partial z}\frac{\partial Q}{\partial z} + \frac{\partial^2 Q}{\partial r^2} + \frac{Q}{4r^2} + K^2 Q = 0. \tag{3}$$

We assume that $r > r_0$, where $k_0 r_0 \gg 1$, and drop the $O(r^{-2})$ term in Eq. (3) to obtain

$$\frac{\partial^2 Q}{\partial z^2} - \frac{1}{\rho}\frac{\partial \rho}{\partial z}\frac{\partial Q}{\partial z} + \frac{\partial^2 Q}{\partial r^2} + K^2 Q = 0. \tag{4}$$

We solve Eq. (4) for $\partial^2/\partial r^2$ in operator notation and take the square root to obtain the outgoing operator

$$\frac{\partial}{\partial r} = ik_0\sqrt{1 + \frac{K^2 - k_0^2 + L}{k_0^2}}, \tag{5}$$

where

$$L = \frac{\partial^2}{\partial z^2} - \frac{1}{\rho}\frac{\partial \rho}{\partial z}\frac{\partial}{\partial z}. \tag{6}$$

We consider a plane wave traveling with the vertical angle $\alpha < \alpha_M$:

$$Q_\alpha = \exp[ik_0(r\cos\alpha + z\sin\alpha)]. \tag{7}$$

Since $\partial Q_\alpha/\partial z = O(\epsilon^{1/2})$ and ρ depends weakly on depth, we are motivated to assume that

$$Q = Q'(z\epsilon^{1/2}), \tag{8}$$

$$\rho = \rho'(z\epsilon^{1/2}), \tag{9}$$

where Q' and ρ' are independent of ϵ. Thus $k_0^{-2}L = O(\epsilon)$ and we may replace the square root in Eq. (5) with its Taylor series approximation to obtain the narrow-angle PE operator

$$\frac{\partial}{\partial r} = ik_0\left(1 + \frac{K^2 - k_0^2 + L}{2k_0^2}\right). \tag{10}$$

Replacing the square root with its Padé approximation, we obtain the wide-angle PE operator

$$\frac{\partial}{\partial r} = ik_0\left(1 + \frac{2(K^2 - k_0^2 + L)}{3k_0^2 + K^2 + L}\right). \tag{11}$$

We define U by

$$Q(r,z) = U(r,z)\exp(ik_0 r). \tag{12}$$

To simplify Eqs. (10) and (11), we assume that $\sigma\beta \ll \epsilon$. For the wide-angle operator, we also require that $k_0^{-1}|k - k_0| \ll \epsilon$ in the water. This assumption, which is valid in shallow water, leads to a TDPE that is easy to solve numerically. Substituting Eq. (12) into Eqs. (10) and (11), we obtain the narrow-angle PE

$$\frac{\partial U}{\partial r} = i(k - k_0)U - \sigma\beta|k_0|U + \frac{iL}{2k_0}U \tag{13}$$

and the wide-angle PE

$$\frac{\partial U}{\partial r} = i(k - k_0)U - \sigma\beta|k_0|U + \frac{2ik_0 L}{4k_0^2 + L}U. \tag{14}$$

Since an outgoing signal is trapped in the water column, Eq. (14) should be valid for wide-angle propagation in shallow water.

We solve Eq. (14) with the method of alternating directions,[17] which requires numerical solutions for each of the following:

$$\frac{\partial U}{\partial r} = i(k - k_0)U, \tag{15}$$

$$\frac{\partial U}{\partial r} = -\sigma\beta|k_0|U, \tag{16}$$

$$4k_0^2\frac{\partial U}{\partial r} + \frac{\partial^3 U}{\partial r\,\partial z^2} - \frac{1}{\rho}\frac{\partial \rho}{\partial z}\frac{\partial^2 U}{\partial r\,\partial z} = 2ik_0\frac{\partial^2 U}{\partial z^2} - 2ik_0\frac{1}{\rho}\frac{\partial \rho}{\partial z}\frac{\partial U}{\partial z}. \tag{17}$$

Equations (15) and (16) can be solved exactly. We apply Galerkin's method to reduce Eq. (17) to

$$R\frac{\partial \mathbf{U}}{\partial r} + S\mathbf{U} = 0, \tag{18}$$

where R and S are tridiagonal matrices and $\mathbf{U}$ is the vector containing the values of U at the depth grid points. This approach is effective for handling piecewise continuous variations in ρ and k.[18] Details regarding the entries of the matrices are given in the Appendix and in Ref. 8. Crank–Nicolson integration is used to solve Eq. (18); Eq. (13) is solved in a similar fashion.

We demonstrate the validity of Eq. (14) and the numerical method with a benchmark problem[19] for which data appear in Table I. Subscripts w and b stand for water and bottom and z_r is the receiver depth. The ocean depth $d = 100$ m is constant. The deep source excites wide-angle modes. Transmission loss data obtained with a normal modes calculation and with Eqs. (13) and (14) using a Gaussian PE starter[3,16] appear in Fig. 1. The results of Eq.

TABLE I. Data for the wide-angle PE benchmark problem. CPU for each PE calculation.

$z_0 = 99.5$ m	$z_r = 99.5$ m	$c_0 = 1500$ m/s
$c_w = 1500$ m/s	$\rho_w = 1$ g/cm^3	$\beta_w = 0$
$c_b = 1590$ m/s	$\rho_b = 1.2$ g/cm^3	$\beta_b = 0.5$ dB/λ
$d = 100$ m	$\omega = 500\pi$ s^{-1}	$\Delta r = 1$ m
$\Delta z = 0.2$ m	$z_M = 200$ m	CPU = 4.5 min

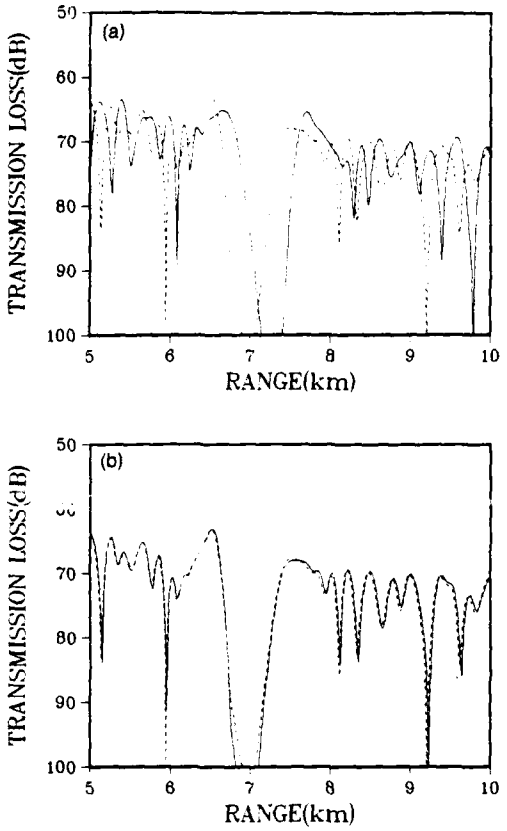

FIG. 1. Wide-angle PE benchmark. Solid curve is (a) narrow-angle PE result and (b) wide-angle PE result. Dashed curve is normal modes result.

(13) exhibit phase delay errors due to wide-angle propagation. The results of Eq. (14) agree well with the normal modes result, which shows that Eq. (14) is a valid wide-angle PE. All calculations were done on a Digital VAX-8650 computer.

II. THE TIME-DOMAIN PARABOLIC EQUATION

We define u by

$$u(r,z,t) = \int_{-\infty}^{\infty} U(r,z,\omega)\exp(-i\omega t)d\omega, \tag{19}$$

$$U(r,z,\omega) = \frac{1}{2\pi}\int_{-\infty}^{\infty} u(r,z,t)\exp(i\omega t)dt. \tag{20}$$

We define $c_0 = \omega/k_0$, rewrite Eq. (13) as

$$\frac{\partial U}{\partial r} = i\omega\left(\frac{1}{c}-\frac{1}{c_0}\right)U - \frac{\sigma\beta|\omega|}{c_0}U + \frac{ic_0L}{2\omega}U, \tag{21}$$

and invert the Fourier transform to obtain the narrow-angle TDPE

$$\frac{\partial u}{\partial r} = \left(\frac{1}{c_0}-\frac{1}{c}\right)\frac{\partial u}{\partial t} + \frac{\sigma\beta}{\pi c_0}\int_{-\infty}^{t}\frac{u(t')-u(t)}{(t'-t)^2}dt' + \frac{c_0L}{2\,\partial/\partial t}u. \tag{22}$$

The integral in Eq. (22) exists as the Cauchy principal value. One can show that the integral operator in Eq. (22) is the inverse transform of the operator $-\sigma\beta|\omega|/c_0$ by verifying it for a single frequency. We rewrite Eq. (14) as

$$\frac{\partial U}{\partial r} = i\omega\left(\frac{1}{c}-\frac{1}{c_0}\right)U - \frac{\sigma\beta|\omega|}{c_0}U + \frac{2i\omega c_0L}{4\omega^2+c_0^2L}U \tag{23}$$

and invert the Fourier transform to obtain the wide-angle TDPE

$$\frac{\partial u}{\partial r} = \left(\frac{1}{c_0}-\frac{1}{c}\right)\frac{\partial u}{\partial t} + \frac{\sigma\beta}{\pi c_0}\int_{-\infty}^{t}\frac{u(t')-u(t)}{(t'-t)^2}dt' + \frac{2c_0(\partial/\partial t)L}{4(\partial^2/\partial t^2)-c_0^2L}u. \tag{24}$$

As for the nonlinear PWE of Ref. 7, each of the terms on the right side of Eq. (24) accounts for a specific physical process; and they are referred to (from left to right) as the refraction term, the attenuation term, and the wide-angle diffraction/density term.

The TDPE can be initialized at $r = r_0$ by the homogeneous half-space field[16]

$$p_h(r,z,t) = \frac{1}{d_-}f\left(t-\frac{d_-}{c_0}\right) - \frac{1}{d_+}f\left(t-\frac{d_+}{c_0}\right), \tag{25}$$

$$d_\pm^2 = r^2 + (z\pm z_0)^2, \tag{26}$$

where $f(t)$ is the source function. The half-space field satisfies the pressure release boundary condition at the ocean surface, and it accounts for the direct arrival and the surface-reflected arrival without accounting for refraction, loss, or bottom reflections. This starter is accurate because refraction and attenuation are weak and can be neglected near the source. Furthermore, rays that reflect from the ocean bottom near the source propagate at large angles. Thus they are not trapped in the oceanic waveguide and do not affect the farfield.

We define $q(r,z,t)$ by $q = r^{1/2}p$ and observe that

$$q(r,z,t) = \int_{-\infty}^{\infty} Q(r,z,\omega)\exp(-i\omega t)d\omega, \tag{27}$$

$$Q(r,z,\omega) = \frac{1}{2\pi}\int_{-\infty}^{\infty} q(r,z,t)\exp(i\omega t)dt, \tag{28}$$

$$u(r,z,t) = \int_{-\infty}^{\infty} Q(r,z,\omega)\exp\left[-i\omega\left(t+\frac{r}{c_0}\right)\right]d\omega. \tag{29}$$

From Eq. (29), we deduce that $u(r,z,t) = q(r,z,t + r/c_0)$. Thus u has the values of q in a reference frame that moves in time and tracks an outgoing signal. In contrast, the PWE involves $v(r,z,t) = q(r + c_0t,z,t)$, where v has the values of q in a reference frame that moves in space.

To solve the TDPE numerically, the source function $f(t)$ is assumed to have compact support. A time window $t_1 < t < t_2$ that contains the signal at all times is chosen. This is possible since the outgoing signal is tracked by the time window. The boundary condition $u = 0$ is used at the pressure release surface, deep within the sediment at $z = z_M$ (from which no energy returns to the water column due to attenuation), and after the signal has passed the observer at $t = t_2$. The boundary conditions $u = \partial u/\partial t = 0$ are used before the signal is detected at $t = t_1$.

We solve the wide-angle TDPE with the alternating directions method with the splitting used to solve the wide-angle PE:

$$\frac{\partial u}{\partial r}+\left(\frac{1}{c}-\frac{1}{c_0}\right)\frac{\partial u}{\partial t}=0, \tag{30}$$

$$\frac{\partial u}{\partial r}=\frac{\sigma\beta}{\pi c_0}\int_{-\infty}^{\infty}\frac{u(t')-u(t)}{(t'-t)^2}\,dt', \tag{31}$$

$$\frac{4}{c_0^2}\frac{\partial^3 u}{\partial r\,\partial t^2}-\frac{\partial^3 u}{\partial r\,\partial z^2}+\frac{1}{\rho}\frac{\partial \rho}{\partial z}\frac{\partial^2 u}{\partial r\,\partial z}=\frac{2}{c_0}\frac{\partial^3 u}{\partial z^2\,\partial t}-\frac{2}{c_0\rho}\frac{\partial \rho}{\partial z}\frac{\partial^2 u}{\partial z\,\partial t}. \tag{32}$$

The Lax–Wendroff method[20] is used to solve Eq. (30), which is a first-order hyperbolic equation.

Since Eq. (16) can be solved exactly, we define the range increment Δr and $\gamma=\sigma\beta\,\Delta r/c_0$ and solve Eq. (31) as follows:

$$U(r+\Delta r,z,\omega)=U(r,z,\omega)\exp(-\gamma|\omega|), \tag{33}$$

$$u(r+\Delta r,z,t)=\int_{-\infty}^{\infty}U(r,z,\omega)\exp(-\gamma|\omega|)\exp(-i\omega t)\,d\omega. \tag{34}$$

Substituting Eq. (20) into Eq. (34) and interchanging the order of integration, we obtain

$$u(r+\Delta r,z,t)=\frac{\gamma}{\pi}\int_{t_1}^{t_2}\frac{u(r,z,t')}{\gamma^2+(t'-t)^2}\,dt'. \tag{35}$$

The kernel of the integral operator of Eq. (35) is large near $t'=t$ because it converges to $\delta(t'-t)$ as $\Delta r\to 0$. This singular behavior makes the operator local and thus numerically efficient. Since the kernel goes to zero rapidly away from $t'=t$, the integration limits can be collapsed to a small interval containing $t'=t$. We approximate the integral over $(t_m-\Delta t/2,\ t_m+\Delta t/2)$ by replacing $u(r,z,t)$ with $u(r,z,t_m)$ and integrating the kernel exactly to obtain

$$u(r+\Delta r,z,t_n)=\frac{1}{\pi}\sum_m\left[\tan^{-1}\left(\frac{t_m-t_n+\frac{1}{2}\Delta t}{\gamma}\right)-\tan^{-1}\left(\frac{t_m-t_n-\frac{1}{2}\Delta t}{\gamma}\right)\right]u(r,z,t_m), \tag{36}$$

where the time grid points are $t_n=n\,\Delta t$ and Δt is the time increment.

Galerkin's method is used to reduce Eq. (32) to

$$A\frac{\partial \mathbf{u}}{\partial r}+B\frac{\partial^3 \mathbf{u}}{\partial r\,\partial t^2}+C\frac{\partial \mathbf{u}}{\partial t}=0, \tag{37}$$

where A, B, and C are tridiagonal matrices and $\mathbf{u}$ is the vector containing the values of u at the depth grid points. Details regarding the entries of these matrices are discussed in the Appendix. Crank–Nicolson integration is used to advance Eq. (37) in range using centered differences in t. Since the energy flow due to geometric dispersion is from t_1 to t_2, it is necessary to sweep from t_1 to t_2.

We demonstrate the validity of Eqs. (22) and (24) with a benchmark.[8] We use the data from Table II with the Gaussian source function

TABLE II. Data for the wide-angle TDPE benchmark problem. CPU for wide-angle TDPF calculation.

$z_0=75$ m	$z_r=25$ m	$c_0=1500$ m/s
$c_w=1500$ m/s	$\rho_w=1$ g/cm^3	$\beta_w=0$
$c_b=1600$ m/s	$\rho_b=1.5$ g/cm^3	$\beta_b=0.5$ dB/λ
$d=d(r)$	$\nu=150$ s^{-1}	$r_0=50$ m
$\Delta r=5$ m	$\Delta z=2$ m	$\Delta t=2/3$ ms
$\omega=100\pi$ s^{-1}	$z_M=300$ m	CPU = 3.75 h

$$f(t)=\exp[-(\nu t)^2], \tag{38}$$

where $\nu=150$ s^{-1}. The ocean depth is 200 m for $r<4$ km, linearly sloping from 200 to 50 m over 4 km $<r<8$ km, and 50 m for $r>8$ km. To prevent reflections, a layer of sediment $100\Delta z$ thick is added below $z=z_M$ in which β increases linearly to 10 dB/λ. We have found this approach effective and use it in all calculations. The results of Eq. (24) appear in Fig. 2. To obtain a sequence of snapshots of the acoustic pressure, we convert the horizontal axis from time to range using the approximation

$$p(r+\delta r,z,t)\cong p(r,z,t-\delta r/c_0), \tag{39}$$

which is valid for small propagation angles and small δr. With this conversion, it is easier to describe the snapshots. The solid contours correspond to $p>0$; the dashed contours correspond to $p<0$.

In the water column, the field consists of a sequence of fronts involving multiple reflections from the ocean surface and bottom. Since the reflection coefficient at the ocean surface is -1 and the reflection coefficient at the ocean bottom is approximately -1 for small-angle incidence, the multiply reflected arrivals alternate between solid and dashed contours. Energy flows to the left due to geometric dispersion. As time increases, the fronts are squeezed together. Large amounts of energy penetrate into the ocean bottom in the upslope region.

The error of the narrow-angle TDPE is analogous to the error of the narrow-angle PE as both involve delays. Distinct features in the narrow-angle transmission loss curve in Fig. 1 appear at larger ranges than they should. For example, the large null that occurs before $r=7$ km appears well beyond $r=7$ km. It is evident from the waveforms appearing in Fig. 3 that energy is dispersed too fast and squeezing is delayed for the narrow-angle TDPE. The errors are small for the first arrivals. However, the agreement gets progressively worse for the later arrivals since the propagation angle increases with arrival time. The agreement improves as wide-angle energy is cut off with decreasing depth.

To obtain a TDPE benchmark, we approximate a time-harmonic source by

$$\sin(\omega t)\cong\sum a^n f(t-t^n), \tag{40}$$

where $\omega=100\pi$ s^{-1}. By superposition, the time-harmonic response p_{cw} is approximated by

$$p_{cw}(r,z,t)\cong\sum a^n p(r,z,t-t^n), \tag{41}$$

where p is the response to f. Details regarding the constants

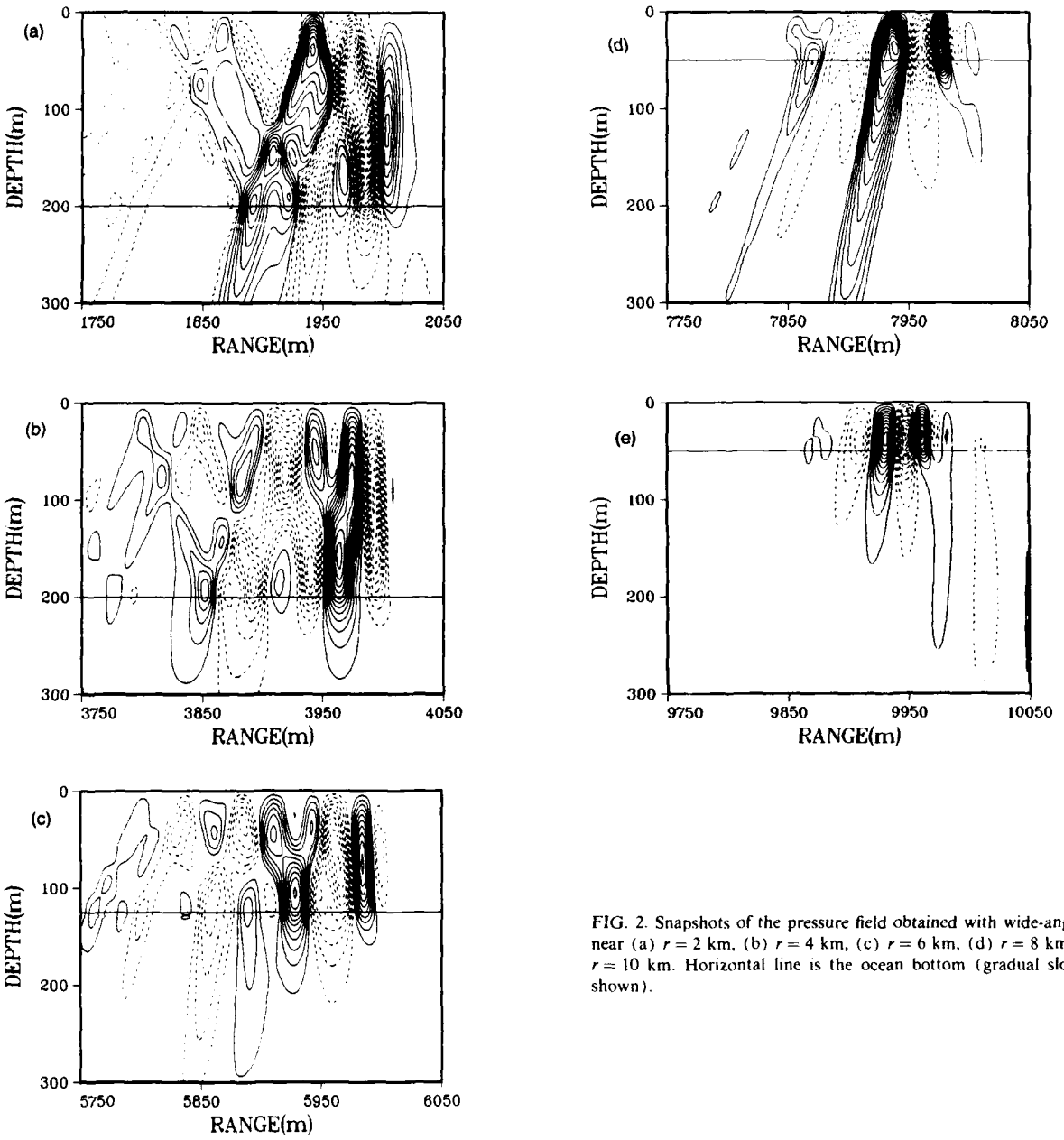

FIG. 2. Snapshots of the pressure field obtained with wide-angle TDPE near (a) $r = 2$ km, (b) $r = 4$ km, (c) $r = 6$ km, (d) $r = 8$ km, and (e) $r = 10$ km. Horizontal line is the ocean bottom (gradual slope is not shown).

a'' and t'' and the approximation of a function by Gaussians are given in Ref. 8. Transmission loss data obtained with Eq. (14) as well as Eqs. (22) and (24) using Eq. (41) appear in Fig. 4. Phase errors are evident for the narrow-angle TDPE calculation. As for the waveforms in Fig. 3, the errors decrease as wide-angle propagation is cut off. The agreement is good for the wide-angle TDPE calculation.

III. COMPARISON OF THE TDPE AND THE PWE

The TDPE and the PWE are special cases of a one-parameter family of methods for solving the wave equation. For $c = \rho = 1$ and $\beta = 0$, the inverse Fourier transform of Eq. (4) is

$$\frac{\partial^2 q}{\partial z^2} + \frac{\partial^2 q}{\partial r^2} = \frac{\partial^2 q}{\partial t^2}. \tag{42}$$

In the derivation of the TDPE, we defined a new dependent variable. In the following analysis, it is convenient to define new independent variables. We introduce $\xi = (t - r)/2$, $\eta = r\cos\phi + t\sin\phi$, and $\zeta = z$, which transform Eq. (42) into

$$\frac{\partial^2 q}{\partial \xi^2} = (\cos\phi + \sin\phi)\frac{\partial^2 q}{\partial \xi\,\partial \eta} + (\cos^2\phi - \sin^2\phi)\frac{\partial^2 q}{\partial \eta^2} = 0. \tag{43}$$

We require that q vanish at $\xi = \xi_0$, $\xi = \xi_0$, and $\zeta = \zeta_1$ and that $\partial q/\partial \zeta$ vanish at $\zeta = \zeta_0$. At $\eta = \eta_0$ we impose the initial condition $q = q_0$. The geometry is illustrated in Fig. 5.

Since the outgoing field is tracked, and it propagates

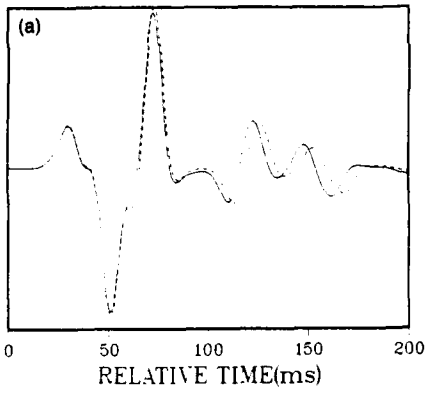

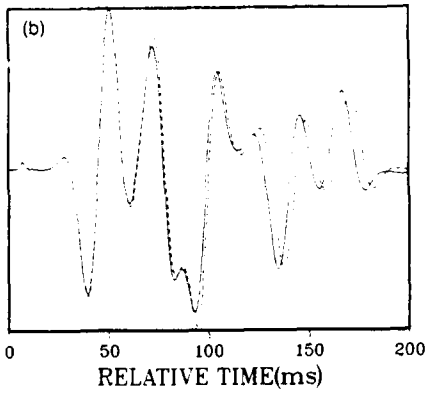

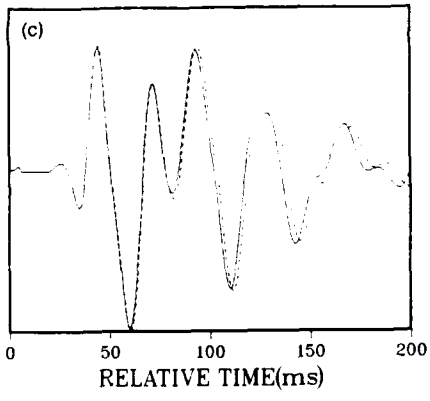

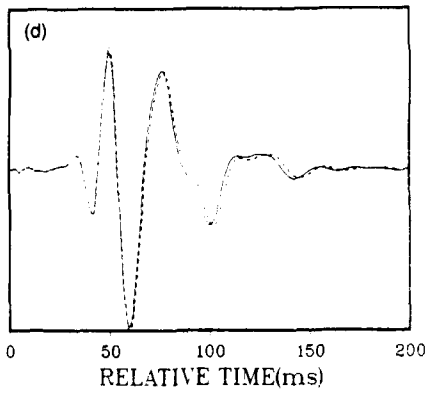

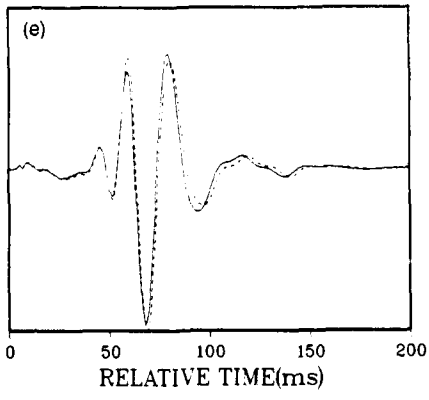

FIG. 3. Waveform detected by receiver at $z = 25$ m and (a) $r = 2$ km, (b) $r = 4$ km, (c) $r = 6$ km, (d) $r = 8$ km, and (e) $r = 10$ km. Solid curve is wide-angle TDPE result. Dashed curve is narrow-angle TDPE result.

with small vertical angles, the dominant operator in Eq. (43) is $\partial/\partial\xi$. Thus we assume that $\partial/\partial\eta \ll \partial/\partial\zeta \ll \partial/\partial\xi$ and drop the third term to obtain

$$\frac{\partial^2 q}{\partial \zeta^2} - (\cos\phi + \sin\phi)\frac{\partial^2 q}{\partial\xi\,\partial\eta} = 0. \tag{44}$$

The narrow-angle TDPE corresponds to $\phi = 0$ in Eq. (44). The narrow-angle PWE corresponds to $\phi = \pi/2$. Thus the narrow-angle TDPE and the narrow-angle PWE have the same canonical form.

Differentiating Eq. (43) with respect to ξ and Eq. (44) with respect to η, we obtain

$$\frac{\partial^3 q}{\partial\xi\,\partial\zeta^2} - (\cos\phi + \sin\phi)\frac{\partial^3 q}{\partial\xi^2\,\partial\eta} + (\cos^2\phi - \sin^2\phi)\frac{\partial^3 q}{\partial\xi\,\partial\eta^2} = 0, \tag{45}$$

$$\frac{\partial^3 q}{\partial\eta\,\partial\zeta^2} - (\cos\phi + \sin\phi)\frac{\partial^3 q}{\partial\xi\,\partial\eta^2} = 0. \tag{46}$$

We solve for $\partial^3 q/\partial\xi\,\partial\eta^2$ in Eq. (46) and substitute the result into Eq. (45) to obtain

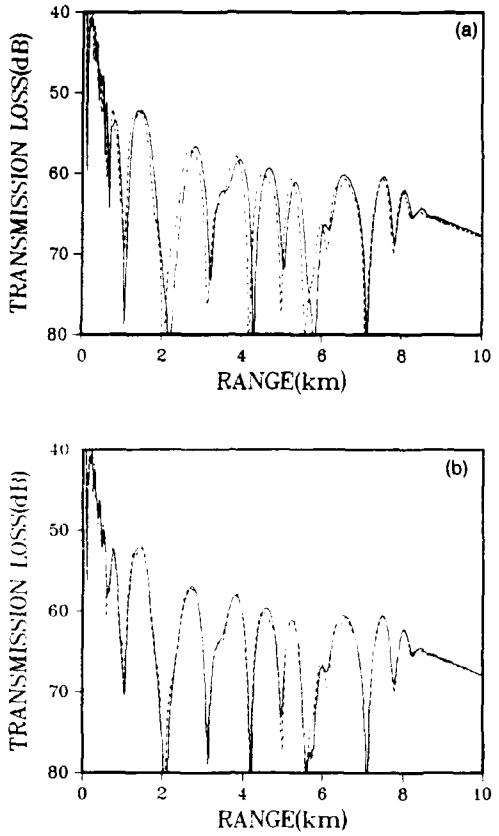

FIG. 4. Wide-angle TDPE benchmark. Solid curve is (a) narrow-angle TDPE result and (b) wide-angle TDPE result. Dashed curve is wide-angle PE result.

$$\frac{\partial^3 q}{\partial\xi\,\partial\zeta^2} - (\cos\phi + \sin\phi)\frac{\partial^3 q}{\partial\xi^2\,\partial\eta} + (\cos\phi - \sin\phi)\frac{\partial^3 q}{\partial\eta\,\partial\zeta^2} = 0. \tag{47}$$

As the sign of the third term changes at $\phi = \pi/4$, the canonical form of Eq. (47) changes.

The wide-angle TDPE is obtained by taking $\phi = 0$ in Eq. (47)

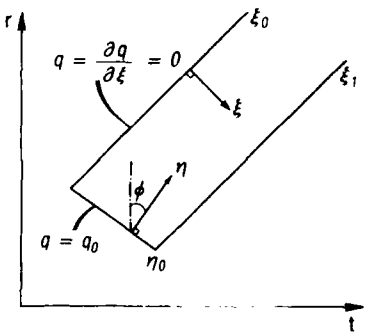

FIG. 5. Geometry of coordinate systems. Signal propagates within the diagonal strip.

$$\frac{\partial^3 q}{\partial\xi\,\partial\zeta^2} - \frac{\partial^3 q}{\partial\xi^2\,\partial\eta} + \frac{\partial^3 q}{\partial\eta\,\partial\zeta^2} = 0. \tag{48}$$

We investigate the stability of Eq. (48) with the energy method.[21] Due to the boundary conditions at $\xi = \xi_0$, Eq. (48) is equivalent to

$$\frac{\partial q}{\partial\eta} = \int_{\xi_0}^{\xi}\frac{\partial^2 q}{\partial\zeta^2}\,d\xi' + \int_{\xi_0}^{\xi}\int_{\xi_0}^{\xi'}\frac{\partial^3 q}{\partial\eta\,\partial\zeta^2}\,d\xi''\,d\xi'. \tag{49}$$

We multiply Eq. (49) by q and integrate over ζ using integration by parts to obtain

$$\frac{\partial}{\partial\eta}\int_{\xi_0}^{\xi_1}\left[\int_{\xi_0}^{\xi}\int_{\xi_0}^{\xi'}\left(\frac{\partial q}{\partial\zeta}\right)^2 d\xi''\,d\xi' + q^2\right]d\zeta = -2\int_{\xi_0}^{\xi}\int_{\xi_0}^{\xi_1}\left(\frac{\partial q}{\partial\zeta}\right)^2 d\zeta\,d\xi'. \tag{50}$$

We define the energy E by

$$E(\xi,\eta) = \int_{\xi_0}^{\xi_1}\left[\int_{\xi_0}^{\xi}\int_{\xi_0}^{\xi'}\left(\frac{\partial q}{\partial\zeta}\right)^2 d\xi''\,d\xi' + q^2\right]d\zeta. \tag{51}$$

Since $\partial E/\partial\eta < 0$ by Eq. (50), we deduce that the wide-angle TDPE is well-posed. A similar argument holds for $\phi < \pi/4$. Thus Eq. (47) is well-posed for $\phi < \pi/4$.

The wide-angle PWE is obtained by taking $\phi = \pi/2$ in Eq. (47)

$$\frac{\partial^3 q}{\partial\xi\,\partial\zeta^2} - \frac{\partial^3 q}{\partial\xi^2\,\partial\eta} - \frac{\partial^3 q}{\partial\eta\,\partial\zeta^2} = 0, \tag{52}$$

$$\frac{\partial}{\partial\eta}\int_{\xi_0}^{\xi_1}\left[\int_{\xi_0}^{\xi}\int_{\xi_0}^{\xi'}\left(\frac{\partial q}{\partial\zeta}\right)^2 d\xi''\,d\xi' - q^2\right]d\zeta = 2\int_{\xi_0}^{\xi}\int_{\xi_0}^{\xi_1}\left(\frac{\partial q}{\partial\zeta}\right)^2 d\zeta\,d\xi'. \tag{53}$$

We define the energy $E = |F|$, where

$$F(\xi,\eta) = \int_{\xi_0}^{\xi_1}\left[\int_{\xi_0}^{\xi}\int_{\xi_0}^{\xi'}\left(\frac{\partial q}{\partial\zeta}\right)^2 d\xi''\,d\xi' - q^2\right]d\zeta. \tag{54}$$

If $F > 0$ initially, $\partial E/\partial\eta > 0$ by Eq. (53). Thus the wide-angle PWE is ill-posed as is Eq. (47) for $\phi > \pi/4$.

To understand why the wide-angle PWE is ill-posed, we replace the initial data at $\xi = \xi_0$ with the boundary data $q = 0$ at $\xi = \xi_0$ and ξ_1. We multiply Eq. (52) by q and integrate over both ζ and ξ using integration by parts to obtain

$$\frac{\partial}{\partial\eta}\int_{\xi_0}^{\xi_1}\int_{\xi_0}^{\xi_1}\left[\left(\frac{\partial q}{\partial\xi}\right)^2 + \left(\frac{\partial q}{\partial\zeta}\right)^2\right]d\xi\,d\zeta = 0. \tag{55}$$

Thus the wide-angle PWE is conservative and well-posed as a two-point boundary value problem for $\phi > \pi/4$. With these boundary conditions, the PWE counterpart of Eq. (32) cannot be solved by sweeping in t making it impractical for numerical calculations.

We now illustrate a problem associated with the fact that the PWE is an initial value problem in time as opposed to range. The maximum range at which p_h may be applied decreases as the source gets closer to the bottom.[16] Thus p_h cannot be used to initialize the field over a wide-range window for a deep source. We modify the problem described in Table II by moving the source down to $z = 180$ m and using the half-space field

$$P_h(r,z) = (1/d_-)\exp(ik_0 d_-) - (1/d_+)\exp(ik_0 d_+) \tag{56}$$

as an initial condition at $r = r_0$. Transmission loss obtained with Eq. (14) appears in Fig. 6 for $r_0 = 50$ and 250 m and for a Gaussian PE starter. The error for the case $r_0 = 250$ m shows that p_h is not valid to 250 m. Based on the waveforms in Fig. 2, which are approximately 250 m in width, a window of this width is reasonable. Thus it would be difficult to construct an initial field for the PWE for this problem. Since the agreement is good for $r_0 = 50$ m, the TDPE can handle this problem using p_h as an initial condition at $r_0 = 50$ m.

IV. DISPERSIVE SEDIMENTS

Dispersion and attenuation are introduced into the TDPE as a perturbation with the definition $K = k + b$, where $b \ll k$ is a complex function of ω. To obtain a TDPE with attenuation and dispersion, the expression $K = k + b$ is substituted into Eq. (23) and the Fourier transform is inverted. This approach allows an arbitrary complex dispersion relation.

Experimental studies involving various materials and frequencies have determined that $\mathrm{Im}(b)$ depends linearly on ω (Refs. 10–12). In a theoretical study,[13] Futterman showed that $\mathrm{Re}(b)$ is determined unambiguously from $\mathrm{Im}(b)$ by the principle of causality and that the following relation between phase velocity c_p and frequency holds:

$$\frac{1}{c_p} = \frac{1}{c} - \frac{2\sigma\beta}{\pi c} \log\left|\frac{\omega}{\omega_0}\right|, \tag{57}$$

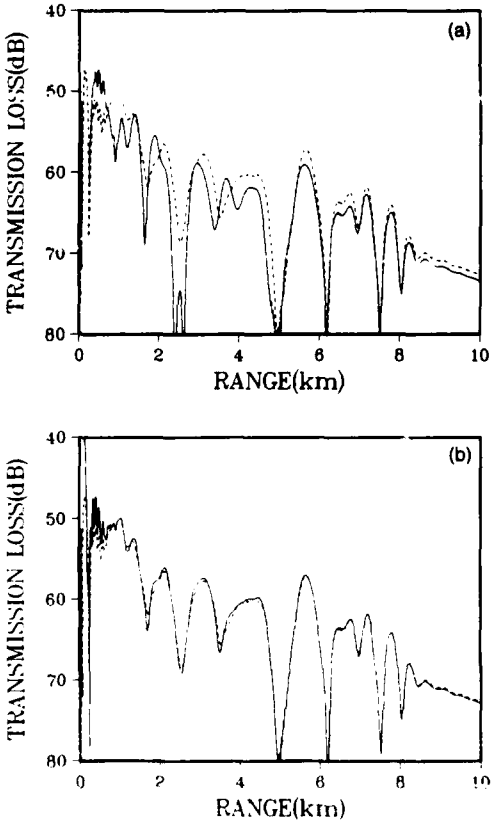

FIG. 6. Wide-angle PE results for deep source. Solid curve obtained with P_h at (a) $r_0 = 250$ m and (b) $r_0 = 50$ m. Dashed curve obtained with Gaussian PE starter.

where ω_0 is a very low reference frequency and $c_p(\omega_0) = c$. Wuenschel showed that the agreement between prediction and observation is excellent if both $\mathrm{Re}(b)$ and $\mathrm{Im}(b)$ are imposed and that the agreement is poor if only $\mathrm{Im}(b)$ is imposed.[11] The effect of sediment dispersion on nearfield acoustic propagation in the ocean has been studied experimentally,[22] and distortions attributed to sediment dispersion were observed in signals received in the sediment. In this article, we are interested in the farfield effects of sediment dispersion on signals received in the water column.

Adding the dispersive term from Eq. (57) to Eq. (23), we obtain

$$\frac{\partial U}{\partial r} = i\omega\left(\frac{1}{c} - \frac{1}{c_0}\right)U - \frac{\sigma\beta|\omega|}{c_0}U - \frac{2i\sigma\beta\omega}{\pi c_0} \times \log\left|\frac{\omega}{\omega_0}\right| U + \frac{2i\omega c_0 L}{4\omega^2 + c_0^2 L}U. \tag{58}$$

Inverting the Fourier transform in Eq. (58), we obtain the wide-angle TDPE with dispersion:

$$\frac{\partial u}{\partial r} = \left(\frac{1}{c_0} - \frac{1}{c}\right)\frac{\partial u}{\partial t} + Mu + \frac{2c_0(\partial/\partial t)L}{4(\partial^2/\partial t^2) - c_0^2 L}u, \tag{59}$$

$$Mu = \frac{-\sigma\beta}{2\pi c_0}\int_{-\infty}^{\infty}\int_{-\infty}^{\infty} u(t')\left(|\omega| + \frac{2i\omega}{\pi}\log\left|\frac{\omega}{\omega_0}\right|\right) \times \exp[i\omega(t'-t)]\,dt'\,d\omega, \tag{60}$$

where M is the attenuation/dispersion operator. The equation

$$\frac{\partial u}{\partial r} = Mu \tag{61}$$

is solved numerically with an approach similar to the approach used to solve Eq. (31). For a single frequency, Eq. (61) has the exact solution

$$U(r + \Delta r, z, \omega) = U(r,z,\omega)\exp\left(-\chi|\omega| - \frac{2i\chi\omega}{\pi}\log\left|\frac{\omega}{\omega_0}\right|\right), \tag{62}$$

where $\chi = \sigma\beta\Delta r/c_0$. The solution of Eq. (61) is obtained by inverting the Fourier transform in Eq. (62) and substituting Eq. (20) for U to obtain

$$u(r + \Delta r, z, t) = \frac{1}{\pi}\int_0^{\infty}\int_{-\infty}^{\infty} u(r,z,t')\exp(-\chi\omega) \times \cos\left[\omega(t'-t) - \frac{2\chi\omega}{\pi}\log\left(\frac{\omega}{\omega_0}\right)\right]dt'\,d\omega. \tag{63}$$

The integral in Eq. (35) is approximated by dividing the time integral into a sum of integrals over small intervals over which u is assumed constant. This approach does not give a robust numerical solution of Eq. (63). Since Eq. (63) accounts for both dispersion and attenuation, it must translate and dampen a waveform. Assuming u constant over each subinterval of time amounts to assuming that u is a step function in time. Thus one might expect this approach to be ineffective because the values at the grid points do not change as a step function propagates a small distance. A robust solution is obtained by approximating u by a parabola over each subinterval.

For $t_m - \Delta t/2 < t' < t_m + \Delta t/2$, we approximate $u(r,z,t')$ with

$$u(r,z,t') \cong u(r,z,t_m) + \frac{u(r,z,t_{m+1}) - u(r,z,t_{m-1})}{2\,\Delta t} \times (t' - t_m) + \frac{u(r,z,t_{m-1}) - 2u(r,z,t_m) + u(r,z,t_{m-1})}{2(\Delta t)^2} \times (t' - t_m)^2. \quad (64)$$

Substituting Eq. (64) in Eq. (63), we obtain the approximate solution

$$u(r + \Delta r,z,t_n) = \sum_m \left\{ F(t_m - t_n)\,u(r,z,t_m) + G(t_m - t_n)\,\frac{u(r,z,t_{m+1}) - u(r,z,t_{m-1})}{2\Delta t} + H(t_m - t_n) \times \frac{u(r,z,t_{m-1}) - 2u(r,z,t_m) + u(r,z,t_{m-1})}{2(\Delta t)^2} \right\}, \quad (65)$$

where

$$F(t) = \frac{2}{\pi} \int_0^\infty \frac{1}{\omega} \exp(-\gamma\omega) \sin\left(\frac{1}{2}\,\omega\,\Delta t\right) \times \cos\left(\omega t - \frac{2\gamma}{\pi}\,\omega \log\frac{\omega}{\omega_0}\right) d\omega, \quad (66)$$

$$G(t) = \frac{1}{\pi} \int_0^\infty \frac{1}{\omega} \exp(-\gamma\omega) \left[\Delta t \cos\left(\frac{1}{2}\,\omega\,\Delta t\right) - \frac{2}{\omega} \sin\left(\frac{1}{2}\,\omega\,\Delta t\right)\right] \sin\left(\omega t - \frac{2\gamma}{\pi}\,\omega \log\frac{\omega}{\omega_0}\right) d\omega, \quad (67)$$

$$H(t) = \frac{1}{\pi} \int_0^\infty \frac{1}{\omega} \exp(-\gamma\omega) \left[\frac{(\Delta t)^2}{2} \sin\left(\frac{1}{2}\,\omega\,\Delta t\right) + \frac{2\Delta t}{\omega} \cos\left(\frac{1}{2}\,\omega\,\Delta t\right) - \frac{4}{\omega^2} \sin\left(\frac{1}{2}\,\omega\,\Delta t\right)\right] \cos\left(\omega t - \frac{2\gamma}{\pi}\,\omega \log\frac{\omega}{\omega_0}\right) d\omega. \quad (68)$$

By manipulating the indices, Eq. (65) becomes

$$u(r + \Delta r,z,t_n) = \sum_{m=m_1}^{m_2} A_m\,u(r,z,t_{m+n}), \quad (69)$$

where the coefficients A_m are easily solved for in terms of F, G, and H. Since the operator converges to $\delta(t' - t)$ as $\Delta r \to 0$, the sum can be collapsed to a small number of grid points near t_n making the operator efficient. The integrals for F, G, and H must be evaluated numerically, but this is a relatively minor task.

To demonstrate the robustness of Eq. (69), we allow it to act on a plane wave with the initial condition

$$u(r_0,z,t) = \sin(\omega_1 t) + 3\sin(\omega_2 t), \quad (70)$$

where $\omega_1 = 100\pi\ \mathrm{s}^{-1}$ and $\omega_2 = 340\pi\ \mathrm{s}^{-1}$. The exact solution is given by

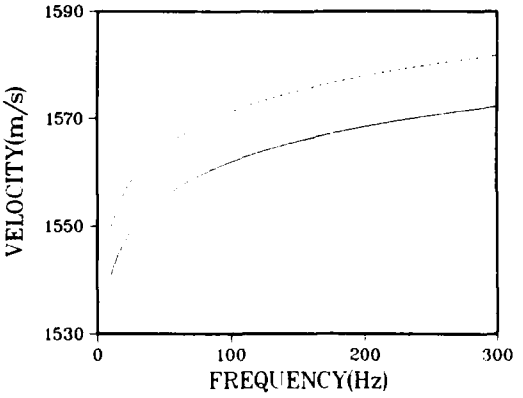

FIG. 7. Solid curve is phase velocity. Dashed curve is group velocity. The difference between the curves is nearly constant.

$$u(r_0 + \Delta r,z,t) = \exp(-\gamma\omega_1)\sin\left(\omega_1 t - \frac{2\gamma}{\pi}\,\omega_1 \log\frac{\omega_1}{\omega_0}\right) + 3\exp(-\gamma\omega_2)\sin\left(\omega_2 t - \frac{2\gamma}{\pi}\,\omega_2 \log\frac{\omega_2}{\omega_0}\right). \quad (71)$$

We let $c = 1520$ m/s, $c_0 = 1500$ m/s, $\beta = 0.5$ dB/λ, $\omega_0 = 2\pi\ \mathrm{s}^{-1}$, $\Delta r = 2$ m, and $\Delta t = 1/3$ ms. The phase and group velocities appear in Fig. 7. It is easy to show from Eq. (57) that the difference between the phase and group velocities is nearly constant over a wide frequency band. The constants A_m appear in Table III for $|m| \leq 20$. In contrast to the constants for the attenuation operator, A_m is negligible for $m > 1$ due to the causality of the attenuation/dispersion operator. We take $m_1 = -20$ and $m_2 = 1$. The results of Eq. (69) appear in Fig. 8 after 100 and 200 range steps. The solution in the absence of dispersion is included for empha-

TABLE III. Coefficients for the numerical solution of the attenuation/dispersion operator. The small numbers in the right column are not used in the calculations.

m	A_m	m	A_m
−20	5.5357370E-05	2	2.0431539E-09
−19	6.3951957E-05	3	3.0856633E-09
−18	7.1207804E-05	4	4.1212398E-09
−17	7.9770936E-05	5	5.1469717E-09
−16	8.9975285E-05	6	6.1596332E-09
−15	1.0226850E-04	7	7.1556476E-09
−14	1.1726187E-04	8	8.1310549E-09
−13	1.3580774E-04	9	9.0814698E-09
−12	1.5912310E-04	10	1.0002032E-08
−11	1.8899402E-04	11	1.0887371E-08
−10	2.2812726E-04	12	1.1731533E-08
−9	2.8078392E-04	13	1.2527930E-08
−8	3.5398538E-04	14	1.3269264E-08
−7	4.5996779E-04	15	1.3947457E-08
−6	6.2160386E-04	16	1.4553552E-08
−5	8.8567595E-04	17	1.5077628E-08
−4	1.3598768E-03	18	1.5508673E-08
−3	2.3321055E-03	19	1.5834473E-08
−2	4.5252889E-03	20	1.5370508E-08
−1	−3.9909109E-02		
0	0.9272352		
1	9.9426970E-02		

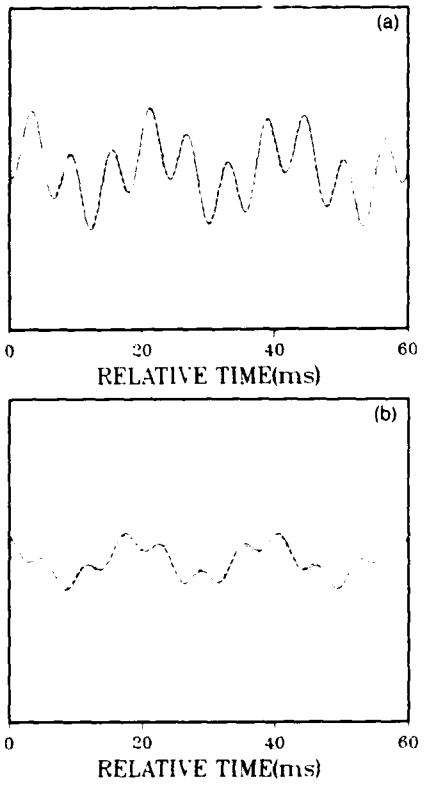

FIG. 8. Benchmark of attenuation/dispersion numerical solution. Solid curve is the numerical solution. Dashed curve is the exact solution. Dotted curve is the exact solution without dispersion term $\mathrm{Re}(b)$, after (a) 100 range steps and (b) 200 range steps.

TABLE IV. Data for the dispersion problem. CPU for TDPE calculation.

$z_0 = 28$ m	$z_s = 28$ m	$c_0 = 1500$ m/s
$c_w = 1500$ m/s	$\rho_w = 1$ g/cm^3	$\beta_w = 0$
$c_b = c_b(\omega, z)$	$\rho_b = 1.5$ g/cm^3	$\beta_b = 0.5$ dB/λ
$d = 30$ m	$\nu = 300$ s^{-1}	$r_0 = 20$ m
$\Delta r = 2$ m	$\Delta z = 1$ m	$\Delta t = 1/3$ ms
$\omega_0 = 2\pi$ s^{-1}	$z_M = 100$ m	CPU = 3.9 h

sis. We observe that the shape of the dispersed wave is distorted. The agreement between the exact and numerical solutions is good.

To demonstrate the effect of sediment dispersion on pulses, we consider the problem described in Table IV. The base sound speed is $c(z) = (1520 + 5z)$ m/s for $z - d < 10$ m, $c(z) = 1570$ m/s for $z - d > 10$ m with $\omega_0 = 2\pi$ s^{-1}. It is evident from Fig. 7 that the phase velocity c_p is about 40 m/s greater than c in a wide frequency band centered about 100 Hz. For comparison, we consider the case with the frequency-independent sediment sound speed $c(z) + 40$ m/s, a sound-speed profile that was assumed in an experimental study.[23] The source is Gaussian with $\nu = 300$ s^{-1}. Contour plots for the solution of Eqs. (24) and (59) appear in Fig. 9. We see from the waveforms in Fig. 10, which is qualitatively similar to Fig. 3 of Wuenschel's paper, that the signal is significantly affected by the dispersion.

It was noted in Ref. 23 that the linear loss law without disperison does not provide good predictions for an environment similar to the one we have just considered, and the linear loss law was challenged. The results in Ref. 23 are

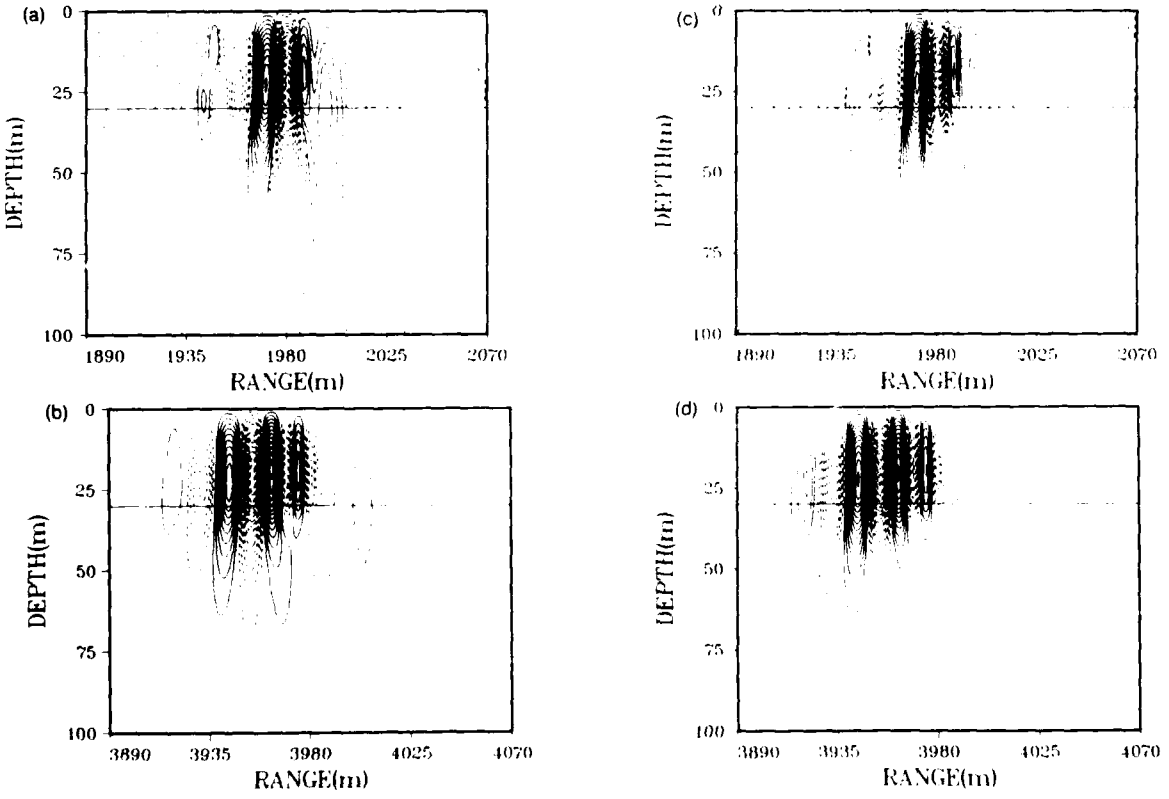

FIG. 9. Snapshots of the pressure field obtained with wide-angle TDPE with dispersion near (a) $r = 2$ km and (b) $r = 4$ km, and with wide-angle TDPE without dispersion near (c) $r = 2$ km and (d) $r = 4$ km.

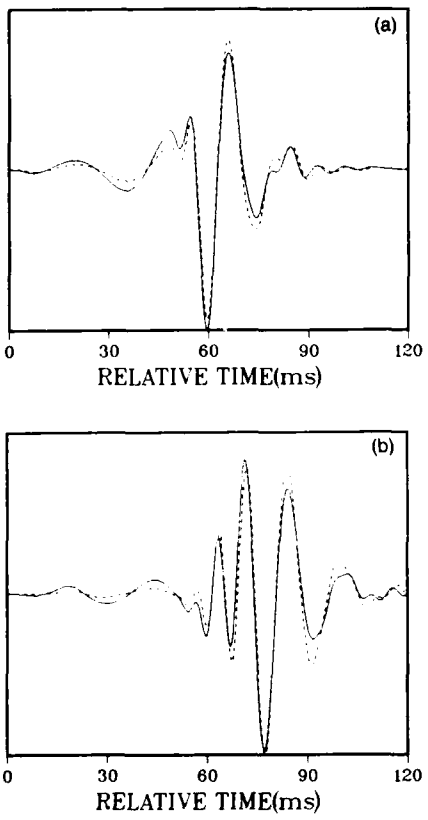

FIG. 10. Waveform detected by receiver at $z = 28$ m and (a) $r = 2$ km and (b) $r = 4$ km. Solid curve is from wide-angle TDPE with dispersion. Dashed curve is from wide-angle TDPE without dispersion.

based on an analysis that neglects sediment dispersion. Based on the results of Wuenschel and the fact that sediment dispersion affects water-borne signals significantly as we have demonstrated, it appears that dispersion might be a better explanation of the observations than a new loss law.

V. CONCLUSIONS

Being the inverse Fourier transform of the PE, the wide-angle TDPE is analytically equivalent to the wide-angle PE. Like the wide-angle PE, the wide-angle TDPE is accurate and efficient and easily handles range-dependent propagation. Since the TDPE is an initial value problem in range, it is easy to construct an accurate initial field for the TDPE. The TDPE handles sediment dispersion, which can have a significant effect on water-borne signals. The TDPE can be initialized with the homogenous half-space field, which is accurate and easy to construct. The numerical solution of the wide-angle TDPE involves the method of alternating directions as well as several other standard numerical methods. The refraction operator is solved with the Lax–Wendroff scheme. The wide-angle diffraction/density operator is solved with the finite element method, centered differences, and Crank–Nicolson integration. The attenuation/dispersion operator is solved with quadrature to evaluate integrals.

ACKNOWLEDGMENTS

This work was supported by the Office of Naval Research and the Naval Ocean Research and Development Activity. The author thanks G. A. Kriegsmann and E. L. Reiss for supporting this work as part of a dissertation at Northwestern University.

APPENDIX: DEPTH DISCRETIZATION WITH GALERKIN'S METHOD

Galerkin's method with linear test functions is applied to discretize depth dependence. We use the approach used in Ref. 8 with some improvements. The depth grid points are defined to be $z_i = i\,\Delta z$, where Δz is the depth increment. The basis functions $\Psi_i(z)$ vanish for $|z - z_i| > \Delta z$, increase linearly from 0 to 1 over $z_{i-1} < z < z_i$, and decrease from 1 to 0 over $z_i < z < z_{i+1}$. The basis functions can be used to approximate a function by a piecewise linear function with exact agreement at the grid points. To solve the wide-angle PE, we define $U_i(r) = U(r,z_i)$, $\Theta = \log(\rho)$, and $\Theta_i = \Theta(z_i)$ to obtain

$$U(r,z) \cong \sum_i U_i(r)\Psi_i(z), \tag{A1}$$

$$\Theta(z) \cong \sum_i \Theta_i \Psi_i(z). \tag{A2}$$

Galerkin's method is used to discretize depth dependence in Eq. (17) by requiring that the following hold for all i:

$$\int \Psi_i(z)\left(4k_0^2\frac{\partial U}{\partial r} + \frac{\partial^3 U}{\partial r\,\partial z^2} - \frac{1}{\rho}\frac{\partial \rho}{\partial z}\frac{\partial^2 U}{\partial r\,\partial z} - 2ik_0\frac{\partial^2 U}{\partial z^2} + 2ik_0\frac{1}{\rho}\frac{\partial \rho}{\partial z}\frac{\partial U}{\partial z}\right) dz = 0. \tag{A3}$$

Equation (18) is obtained by substituting Eqs. (A1) and (A2) into Eq. (A3). The entries of the matrices R and S are determined by the following approximations obtained with Galerkin's method:

$$\left.\frac{\partial^2 U}{\partial z^2}\right|_{z=z_i} \cong \frac{U_{i-1} - 2U_i + U_{i+1}}{(\Delta z)^2}, \tag{A4}$$

$$U|_{z=z_i} \cong \frac{U_{i-1} + 4U_i + U_{i+1}}{6}, \tag{A5}$$

$$\left.\frac{\partial \Theta}{\partial z}\frac{\partial U}{\partial z}\right|_{z=z_i} \cong \frac{(2\Theta_i - \Theta_{i-1} - \Theta_{i+1})U_i}{2(\Delta z)^2} + \frac{(\Theta_{i-1} - \Theta_i)U_{i-1} + (\Theta_{i+1} - \Theta_i)U_{i+1}}{2(\Delta z)^2}. \tag{A6}$$

The entries of the matrices A, B, and C are also derived from the above difference formulas.

[1] M. D. Collins, "Benchmark Calculations for Higher-Order Parabolic Equations," J. Acoust. Soc. Am. (submitted).
[2] "NORDA Parabolic Equation Workshop," edited by J. A. Davis, D. White, and R. C. Cavanagh, NORDA Tech. Note 143 (1982).
[3] F. D. Tappert, "The Parabolic Approximation Method," in *Wave Propagation and Underwater Acoustics*, edited by J. B. Keller and J. S. Papadakis, Lecture Notes in Physics, Vol. 70 (Springer, New York, 1977).

[4]J.F. Claerbout, *Fundamentals of Geophysical Data Processing* (McGraw-Hill, New York, 1976), pp. 206–207.
[5]G. Botseas, D. Lee, and K. E. Gilbert, "IFD: Wide-Angle Capability," NUSC Tech. Rep. 6905 (1983).
[6]Reference 4, pp. 208–215.
[7]B. E. McDonald and W. A. Kuperman, "Time Domain Formulation for Pulse Propagation Including Nonlinear Behavior at a Caustic," J. Acoust. Soc. Am. **81**, 1406–1417 (1987).
[8]M. D. Collins, "Low-Frequency, Bottom-Interacting Pulse Propagation in Range-Dependent Oceans," IEEE J. Ocean. Eng. **13**(4), 222–228 (1988).
[9]J. F. Murphy, "Finite-Difference Treatment of a Time-Domain Parabolic Equation: Theory," J. Acoust. Soc. Am. **77**, 1958–1960 (1985).
[10]F. J. McDonal, F. A. Angona, R. L. Mills, R. L. Sengbush, R. G. Van Nostrand, and J. E. White, "Attenuation of Shear and Compressional Waves in Pierre Shale," Geophysics **23**, 421–439 (1958).
[11]P. C. Wuenschel, "Dispersive Body Waves—An Experimental Study," Geophysics **15**, 539–551 (1965).
[12]E. L. Hamilton, "Compressional-Wave Attenuation in Marine Sediments," Geophysics **37**, 620–646 (1972).
[13]W. I. Futterman, "Dispersive Body Waves," Geophys. Res. **67**, 5279–5291 (1962).
[14]A. D. Pierce, "Augmented Adiabatic Mode Theory for Upslope Propagation from a Point Source in Variable-Depth Shallow Water Overlying a Fluid Bottom," J. Acoust. Soc. Am. **74**, 1837–1847 (1983).
[15]P. G. Bergmann, "The Wave Equation in a Medium with a Variable Index of Refraction," J. Acoust. Soc. Am. **17**, 329–333 (1946).
[16]M. D. Collins, "A Near-Field Asymptotic Analysis for Underwater Acoustics," J. Acoust. Soc. Am. (submitted).
[17]A. R. Mitchell and D. F. Griffiths, *The Finite Difference Method in Partial Differential Equations* (Wiley, New York, 1980), pp. 59–70.
[18]K. E. Gilbert, "A Finite Element Method for the Parabolic Wave Equation," in Ref. 2, p. 81.
[19]Reference 2, pp. 46–57.
[20]Reference 17, pp. 167–168.
[21]Reference 17, pp. 44–47.
[22]D. J. Wingham, "The Dispersion of Sound in Sediment," J. Acoust. Soc. Am. **78**, 1757–1760 (1985).
[23]J. Zhou, X. Zhang, P. H. Rogers, and J. Jarzynski, "Geoacoustic Parameters in a Stratified Sea Bottom from Shallow-Water Acoustic Propagation," J. Acoust. Soc. Am. **82**, 2068–2074 (1987).

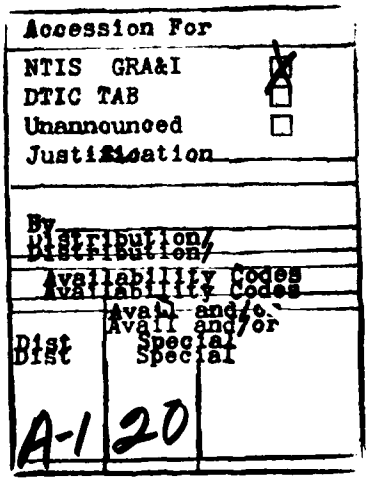

REPORT DOCUMENTATION PAGE

Form Approved
OMB No. 0704-0188

1a. REPORT SECURITY CLASSIFICATION Unclassified	1b. RESTRICTIVE MARKINGS None
2a. SECURITY CLASSIFICATION AUTHORITY	3. DISTRIBUTION/AVAILABILITY OF REPORT Approved for public release; distribution is unlimited.
2b. DECLASSIFICATION/DOWNGRADING SCHEDULE	
4. PERFORMING ORGANIZATION REPORT NUMBER(S) JA 244:036:88	5. MONITORING ORGANIZATION REPORT NUMBER(S) JA 244:036:88
6a. NAME OF PERFORMING ORGANIZATION Naval Ocean Research and Development Activity 6b. OFFICE SYMBOL (If applicable) 221	7a. NAME OF MONITORING ORGANIZATION Ocean Acoustics and Technology Directorate Naval Ocean Research and Development Activity
6c. ADDRESS (City, State, and ZIP Code) Stennis Space Center, MS 39529-5004	7b. ADDRESS (City, State, and ZIP Code) Stennis Space Center, MS 39529-5004
8a. NAME OF FUNDING/SPONSORING ORGANIZATION Naval Ocean Research and Dev. Act. 8b. OFFICE SYMBOL (If applicable) 244	9. PROCUREMENT INSTRUMENT IDENTIFICATION NUMBER
8c. ADDRESS (City, State, and ZIP Code) Stennis Space Center, MS 39529-5004	10. SOURCE OF FUNDING NUMBERS PROGRAM ELEMENT NO.: 6115N PROJECT NO.: 03205 TASK NO.: 330 WORK UNIT ACCESSION NO.: 12219B-00

11. TITLE (Include Security Classification)

The time-domain solution of the wide-angle paragolic equation including the effects of sediment dispersion

12. PERSONAL AUTHOR(S)

Michael D. Dollins

13a. TYPE OF REPORT	13b. TIME COVERED	14. DATE OF REPORT (Year, Month, Day)	15. PAGE COUNT
Journal Article	FROM _____ TO _____	1988, December	12

16. SUPPLEMENTARY NOTATION

17. COSATI CODES			18. SUBJECT TERMS (Continue on reverse if necessary and identify by block number)
FIELD	GROUP	SUB-GROUP	time-domain, parabolic equation, wide-angle, sediment dispersion

19. ABSTRACT (Continue on reverse if necessary and identify by block number)

The wide-angle time-doamin parabolic equation (TDPE), which is the inverse Fourier transform of the wide-angle parabolic equation (PE), is derived. A numerical solution for the model is described and a benchmark calculation is presented. The narrow-angle PE. The TDPE is compared with the progressive wave equation, which is shown to be restricted to narrow-angle propagation for practical purposes. In the sediment, attenuation is assumed to depend linearly on frequency and the corresponding causal dispersion law is assumed. The model is used to show that the effect of sediment dispersion on pulse propagation in the ocean can be significant.

20. DISTRIBUTION/AVAILABILITY OF ABSTRACT	21. ABSTRACT SECURITY CLASSIFICATION	
☐ UNCLASSIFIED/UNLIMITED ☒ SAME AS RPT. ☐ DTIC USERS	Unclassified	
22a. NAME OF RESPONSIBLE INDIVIDUAL Michael D. Collins	22b. TELEPHONE (Include Area Code) 601 688-5583	22c. OFFICE SYMBOL 221

DD Form 1473, JUN 86 *Previous editions are obsolete.*